Electronic Supplementary Material (ESI) for Nanoscale.

SUPPLEMENTARY INFORMATION

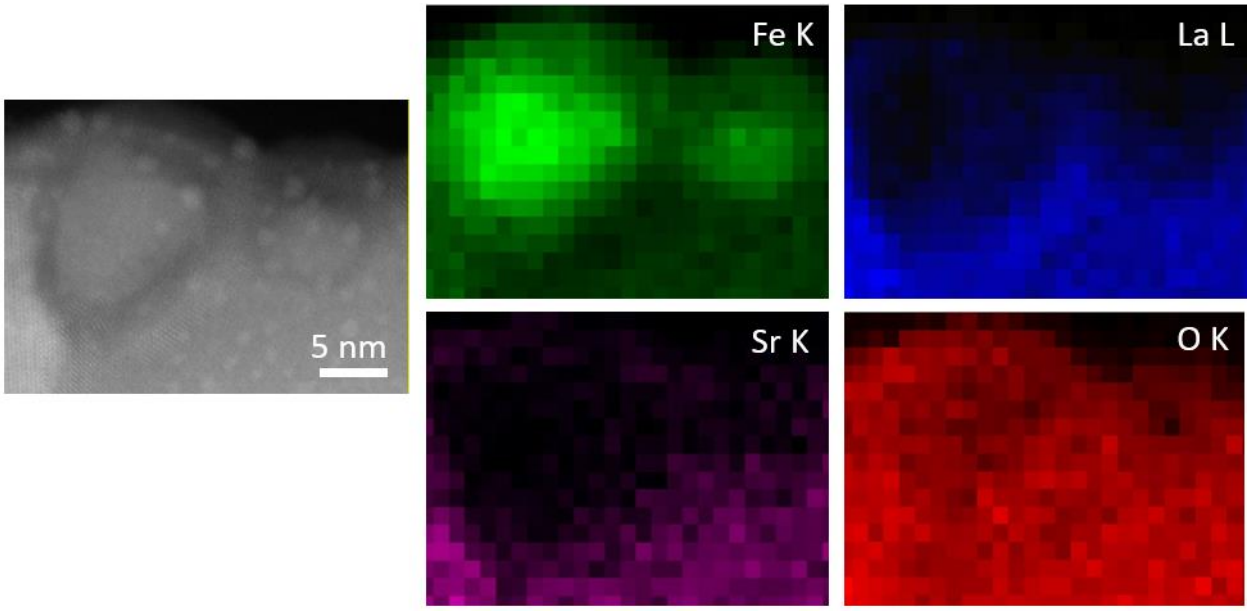

Fig. S1: STEM HAADF image of surface core-shell nanostructure and corresponding elemental EDS maps of Fe K, La L, Sr K and O K.

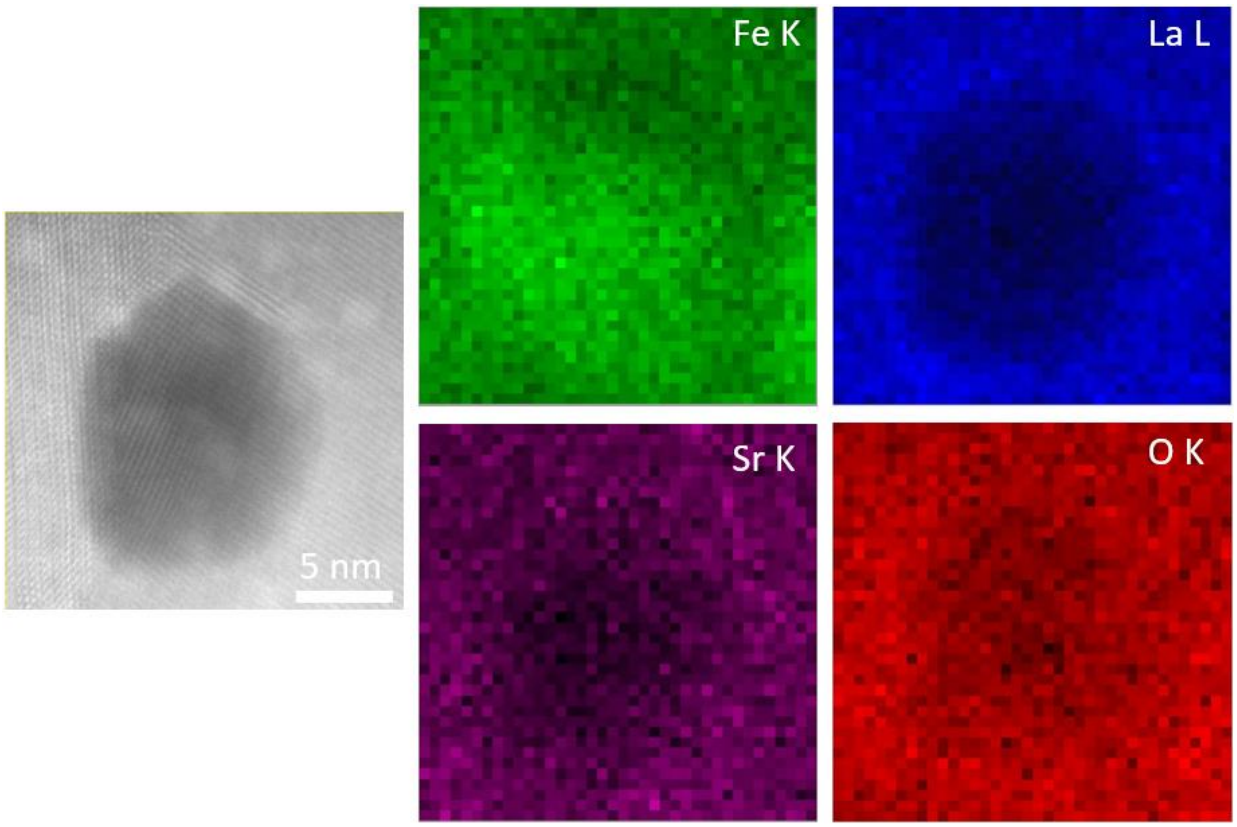

Fig. S2: STEM HAADF image of bulk core-shell nanostructure and corresponding elemental EDS maps of Fe K, La L, Sr K and O K.

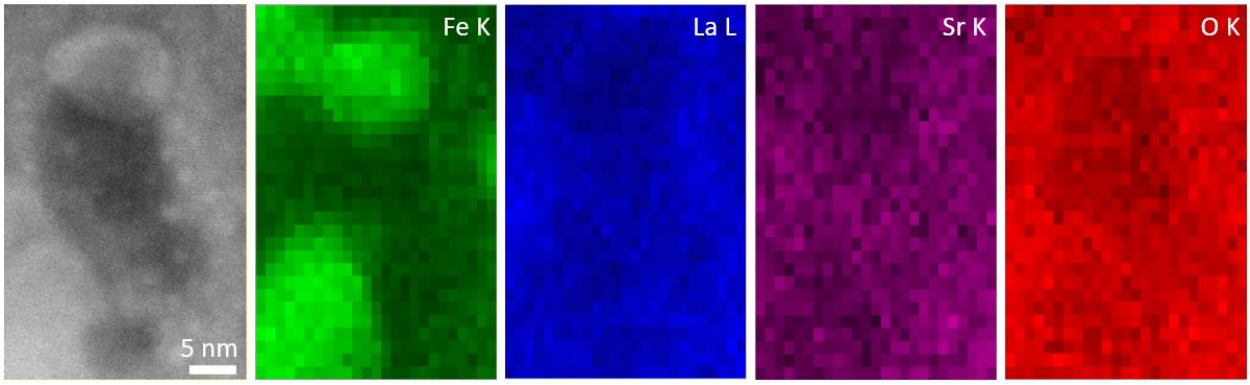

Fig. S3: STEM HAADF image of adjacent Fe-rich and Fe-depleted nanostructures and corresponding elemental EDS maps of Fe K, La L, Sr K and O K.

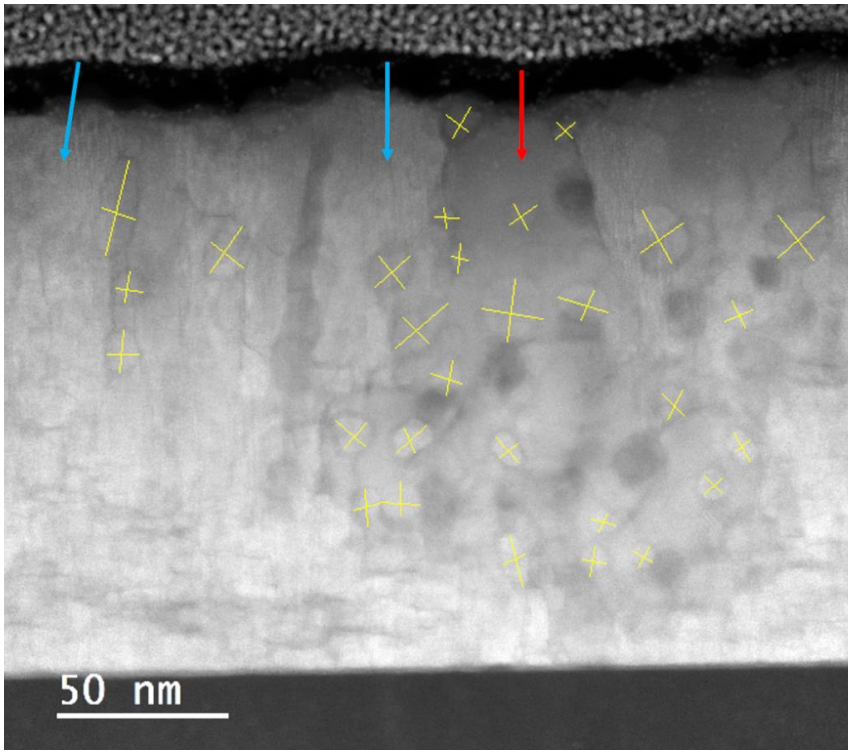

Fig. S4: STEM HAADF image showing markings for major axis 'a' and minor axis 'b' dimensions of the ellipsoidal particles in LSF exsolved film used for calculations of average size of Fe nanostructures and shape factor. Blue arrows mark some of the LSF_{214} (RP) domains. Red arrows mark the LSF_{113} matrix region.

Fe exsolution mechanism was studied in a model single-crystal LSF thin film:

A model thin film of LSF, ~20 nm, was grown epitaxially on Nb-doped STO to investigate atomic-scale properties of exsolved thin films to complement observations of relatively 'thick' LSF films (~165 nm). The thin film of LSF/Nb:STO was reduced at 650 ^{o}C in 3% H_2/N_2. More details of the thin film deposition can be found elsewhere[6].The STEM EDS and EELS data of the model LSF thin film is obtained with a probe-corrected STEM operating at 200 kV (JEOL Grand ARM 200F at Harvard University equipped with a Gatan Enfinium energy-loss spectrometer capable of dual EELS). The EELS data presented and used for analysis here were acquired using a 2D spectrum image, and represent the sum of ~ 35 spectra each acquired with an acquisition time of 0.01 s. The EEL spectrometer entrance aperture diameter was 5 mm, and the dispersion was 1 eV. EEL spectra were calibrated by aligning the La M_5 peak (830 eV), and background subtraction was performed by extrapolation of the inverse power law function fitted to the Fe L_{23} and La M_{45} pre-edge signals. After background subtraction, the intensity of the Fe and La core-loss signals were calculated via integration within the signal integration windows provided in table 1. The zero-loss peak was recorded at each pixel position in the spectrum image, and the specimen thickness was ~ 0.15 inelastic mean free paths.

Table S1: Parameters used for EELS data fitting

	Fe L_{23}	La M_{45}
Background fitting window (eV)	617 – 684	748 – 815
Signal integration window (eV)	748 – 815	816– 866

RP mosaic structures [64,65] containing Fe-depleted planar defects were observed following Fe exsolution from a model epitaxial LSF thin film. The defect structures, so-called RP mosaics (Fig. S5), have been detailed previously by Suzuki *et al.* [64] and observed again by Brooks *et al.* [65] while studying A-site-excess $SrTiO_3$. Following thermochemical exsolution treatment, Fe oxide particles were observed partially submerged in the surface of the LSF thin film, shown elsewhere[6].

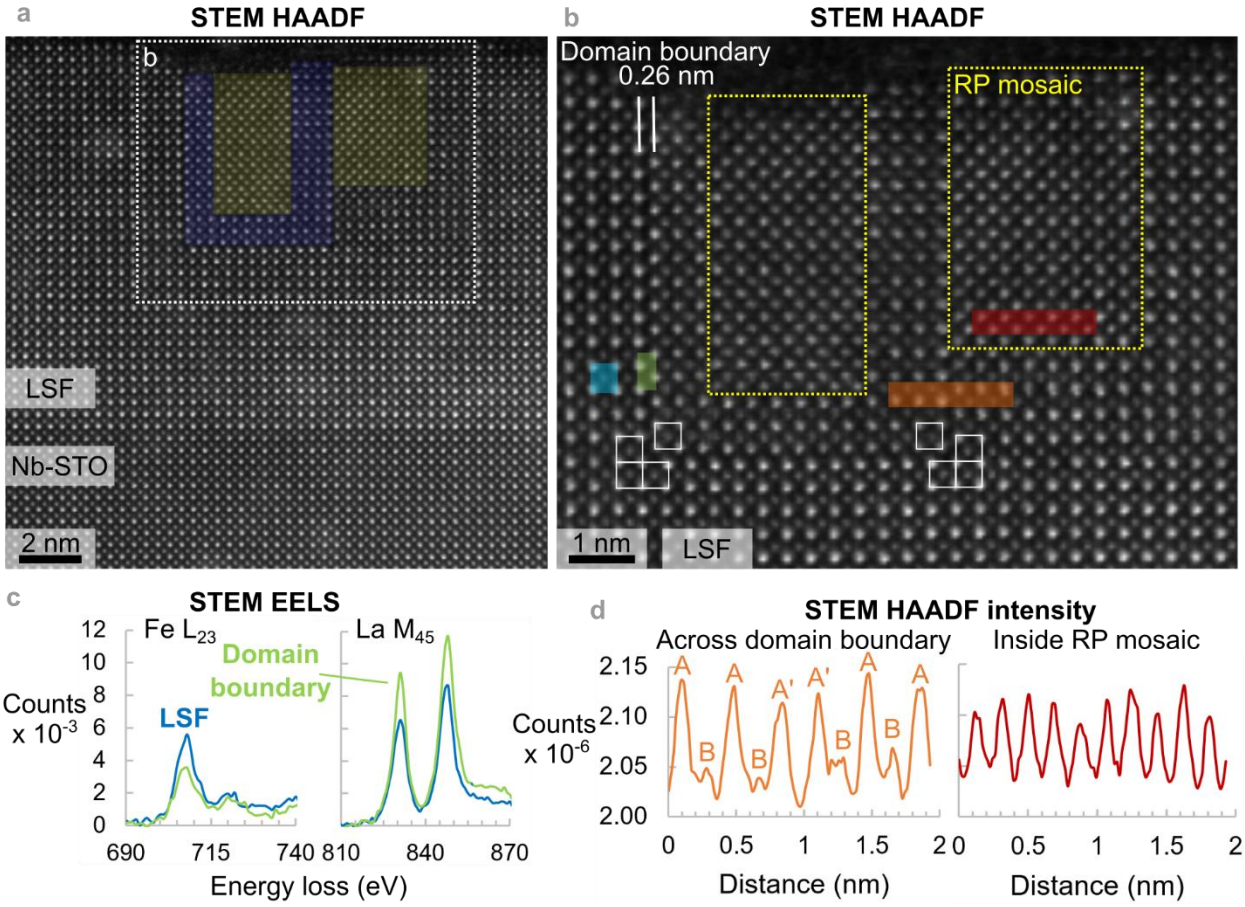

Fig. S5: Atomic-scale characterization of RP domains. (a) STEM HAADF image of Ruddleson-Popper domains in LSF (type 1 domain highlighted in blue and RP mosaics in yellow). (b) Expanded view of the RP domain boundary showing A-site terminations (type-1 domain corners are indicated by white squares). RP mosaic regions show overlap between displaced domains and LSF matrix. (c) Core-loss EELS of Fe L_{23} and La M_{45} acquired from the LSF matrix (blue) and the domain boundary (green) regions highlighted blue and green in (b), respectively. The background subtracted signals were acquired from two regions of (0.246 nm)^2. (d) STEM HAADF intensity profiles from a domain boundary and from inside a RP mosaic; profiles were calculated in the regions highlighted orange and red, respectively. Unlike at the domain boundary, atomic number (Z) contrast between A- and B- sites is not visible in the RP mosaic.

Atomic resolution STEM imaging and EELS analysis suggest that Fe may be diffusing along {001} planes during exsolution, causing Fe deficiency in these planes and the formation of RP

mosaic structures. Similar to the description provided by Suzuki *et al.*, we observed two types of embedded domains. The first type has the perovskite structure but is displaced relative to the LSF matrix by ½a[110] (blue region in Fig. S5a). Between the LSF and type-1 domain there is a domain boundary along {001} planes. The domain boundary consists of two A-site terminations (Fig. S5b) with a (001) interplanar spacing of 0.26 nm +/- 0.02 nm, reduced from 0.36 +/- 0.02 nm in the LSF (uncertainty is width of one pixel; Fig. S5b). The A-A domain boundary is evident in the integrated HAADF intensity profile (Fig. S5d) calculated in the orange region of Fig. S5b. The second domain type also has the symmetry of the LSF perovskite matrix (yellow regions in Fig. S5a, and boxed regions of Fig. S5b). However, the HAADF intensity at the A- and B-sites is nearly equal (Fig. S5d), indicating that the mean atomic number in each atomic column is approximately equal. Thus, the HAADF image of these RP mosaics (Fig. S5b) is thought to be a projection of type-1 domains overlapping with the LSF matrix.

The 0.26 nm A-A domain boundary was Fe-depleted relative to the LSF matrix and RP domains, and there was a significant amount of Fe^{2+} in the domain. STEM core-loss EELS analysis of the LSF matrix (blue curve in Fig. S5c) and domain boundary (green curve) revealed a decrease in the Fe L_{23} signal and an increase in the La M_{45} signal in the domain boundary. Comparison of the Fe L_{23} EELS near-edge fine structure measured in the LSF and in the domain boundary revealed a 1-eV shift of the Fe L_3 peak (~ 704 eV) to lower energy loss in the domain, indicative of appreciable Fe reduction from 3+ to 2+ (Fig. S5c).